[14] J. T. Weaver and C. R. Brewitt-Taylor, "Improved boundary conditions for the numerical solution of E-polarization problems in geomagnetic induction," *Geophys. J. Roy. Astron. Soc.*, vol. 54, pp. 309-317, 1978.

[15] T. W. Dawson and J. T. Weaver, "H-polarization induction in two thin half-sheets," *Geophys. J. Roy. Astr. Soc.*, vol. 56, 1979.

[16] G. Fischer, "Electromagnetic induction effects at an ocean coast," in *Proc. IEEE*, this issue, pp. 1050-1060.

[17] C. R. Brewitt-Taylor and J. T. Weaver, "On the finite difference solution of two-dimensional induction problems," *Geophys. J. Roy. Astron. Soc.*, vol. 47, pp. 375-396, 1976.

[18] T. W. Dawson and J. T. Weaver, "Three-dimensional induction in a non-uniform thin sheet at the surface of a uniformly conducting earth," manuscript in preparation, 1979.

[19] F. W. Jones and J. E. Lokken, "Irregular coastline and channeling effects in three-dimensional geomagnetic perturbation models," *Phys. Earth Planet. Inter.*, vol. 10, pp. 140-150, 1975.

[20] R. P. Ranganayaki and T. R. Madden, "A generalized thin sheet model and its application to a study of ocean-continent edge effects," presented at *4th Workshop Electromagnetic Induction in the Earth and Moon* (Murnau, Germany, Sept. 7-13, 1978).

# Electromagnetic Induction Effects at an Ocean Coast

GASTON FISCHER

*Invited Paper*

*Abstract*—This paper reviews recent progress in model calculations towards understanding electromagnetic induction effects at ocean coasts. Early models consisted of two adjacent quarter-spaces of different conductivity, whereas the newer models simulate the ocean with a very thin sheet of a perfect conductor placed on top of a uniform Earth medium. The inducing field is assumed to arise from a monochromatic plane wave incident vertically from above. With any of these models one succeeds at once in explaining the occurrence of large vertical magnetic fields when the inducing electric field is polarized parallel to the coast (*E*-polarization), thereby also confirming the highly directional character of the coast effects as discovered a few years before by Parkinson. Another important step was made when, first numerically, then analytically, the behavior of the horizontal component of the magnetic field at the surface was rigorously calculated. For *H*-polarization (inducing magnetic field parallel to shore) this horizontal surface field is uniform, but is not so for *E*-polarization. Indeed, it has now been shown that the surface field can vary appreciably close to the coast, particularly on the ocean side of shore. With *E*-polarization, very large currents flow in the ocean, parallel to shore, with the result that the effect of the coast is felt at very large distances over both land and sea. Under *H*-polarization induction the range of the coast effect is very much shorter, in fact almost an order of magnitude shorter over the land and even reducing to zero at the surface of the perfectly conducting model ocean. The magnetic fields at the ocean floor have also been calculated, which should be of interest in the rapidly expanding field of marine survey and prospecting.

## I. Introduction and Historical Remarks

INTEREST in the possible effect of oceans on the Earth's magnetic field dates back to the middle of the last century (cf. the review by Bullard and Parker [1]), although the occurrence of unusual electromagnetic induction effects at ocean coasts has, in fact, been recognized in the records of geomagnetic coastal stations in the past thirty years only. These rather recent observations were made in purely natural phenomena and before any effect was sought in problems of wave propagation. What was seen mainly were unusually large variations of the local vertical component of the Earth's magnetic field, when stations far inland were taken for comparison. It is not surprising, therefore that the first theoretical attempts to understand the coast effect concentrated on these vertical field variations. At this point we may note that for a horizontally layered flat Earth and a uniform primary field, no vertical variation is induced.

In 1970, Bullard and Parker [1] were still rather pessimistic in their appraisal of attempts toward a theoretical understanding of the ocean coast effect. We believe that some significant progress, which it is precisely our aim to review here, has recently been made in this direction. Many particular or local seacoast problems remain to be studied, but the main ocean-coast effect is probably reasonably well-understood today.

Many ocean-coast models that have been studied consist of thin sheet conductors only. We will not consider this subject here, referring the interested reader to the review by Ashour [2]. The coast models we will be looking at instead are non-uniform conducting structures making up an entire half-space, and the scale of these structures will be intermediate, i.e., neither very local nor global. What we mean by this statement is that we will neglect both the curvature of the Earth and any surface topography, considering the upper surfaces of both land and oceans as a common horizontal plane. There are of course ocean coast problems of a continental scale, where the curvature of the Earth is of utmost importance, but we shall

Manuscript received June 26, 1978; revised October 11, 1978. This paper was presented at the URSI General Assembly, Helsinki, Norway, July 31 to August 10, 1978. This work was supported in part by a Grant from the Swiss National Science Foundation.

The author is with the Observatoire Cantonal, CH-2000 Neuchâtel, Switzerland.

0018-9219/79/0700-1050$00.75 

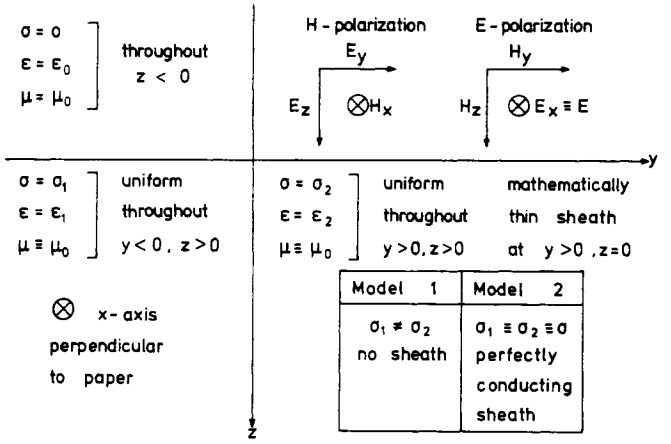


**Fig. 1. Cross section of two model structures of an ocean coast. In model 1 the ocean is the region where $\sigma = \sigma_2 >> \sigma_1$. In model 2 the ocean is simulated by a mathematically thin but perfect conductor at ($y > 0$, $z = 0$). For $H$-polarization induction only components $E_y$, $E_z$, and $H_x$ occur. With $E$-polarization only $E_x$, $H_y$, and $H_z$ are induced.**

not look at these problems here. We will also assume that the inducing field is uniform. Again this limits our scale of lengths to say, less than 1000 km, since this assumption of uniformity implies that the sources of the fields are at very large distances, and in general means that we are looking at natural phenomena. This assumed uniformity is of course seldom truly realized in nature, but on the length-scale that we consider here the source location is generally not stable in time, and our assumption is therefore reasonably well justifed in the statistical sense. In addition to the upper limit of lengths mentioned, a lower limit is set by our neglect of any surface topography as well as by the assumption, made in many a theoretical calculation, that displacement currents can be neglected, i.e., that $\omega\epsilon\rho \ll 1$. Here $\rho = 1/\sigma$ is the resistivity, $\epsilon = \chi_e\epsilon_0$ the dielectric constant, and $f = \omega/2\pi$ the frequency. Obviously, the range of lengths that we will consider corresponds to a range of frequencies or periods $T$, and these ranges will be determined by the resistivities we have to deal with. For a typical rock resistivity of $\rho = 100\ \Omega$m, the range of lengths may extend from 10 m to 1000 km and the range of periods from $10^{-6}$ s to 10 h.

Noticing the unusually large vertical magnetic field variations was only a first step toward the full understanding of the ocean coast effect. A real breakthrough occurred when Parkinson [3]-[5] (cf. also Wiese [6]) observed that these variations had a highly directional character, in the sense that the vertical variations were almost totally correlated with those horizontal variations which are perpendicular to the coastline and not correlated with magnetic field variations parallel to the coast. This led Parkinson [3]-[5] and Wiese [6] to propose their now famous arrow representation, which generated a flurry of papers confirming their discovery. The original arrow concept was later refined when it was recognized that the character of the in-phase correlation was somewhat different from the out-of-phase or quadrature correlation [7a].

The directional nature of the correlation between vertical and horizontal variation is a direct consequence of the essentially two-dimensional (2-$D$) nature of most ocean coasts, i.e., the invariance of the coast profile with regard to translations parallel to the shoreline. Fig. 1 illustrates this translational invariance for two particular ocean coast models. For 2-$D$ structures, Weaver [8] and Fischer [9] independently showed that the electromagnetic response separates into two independent modes, according to whether the incident wave has its magnetic vector $H$ parallel ($H$-polarization induction) or perpendicular ($E$-polarization induction) to the coastline. Fig. 1 shows which field components are induced in these two independent modes, and it becomes at once evident that the vertical component $H_z$ can only be connected with $H_y$, the component perpendicular to shore. In his paper, Weaver [8] set out to understand the coast effect by solving an ocean coast model consisting of two adjacent quarter-spaces (cf. Fig. 1). Although Weaver's original $E$-polarization solution [8] was shown later [10], [11] to be only a first approximation, it was quite successful in its goal of explaining the coast effect theoretically, at least as concerns the vertical magnetic field.

The fact that Weaver's [8] original $H$-polarization solution was quite rigorous, whereas his $E$-polarization solution was not, is of interest and relates to another important hurdle in the way of a complete understanding of the ocean coast effect. Looking at Fig. 1, one easily perceives that with $H$-polarization induction the current streamlines can but go from left to right or vice versa. Since the upper half-space ($z < 0$) is nonconducting, arguments of continuity require that the current integrated from $z = 0$ to $z = +\infty$ be independent of coordinate $y$ (as will be seen below this statement is correct only within the quasi-static limit). Consequently, and with Maxwell's equations, the magnetic field at the surface is also independent of coordinate $y$. Because of the translational invariance it follows that this field is uniform in the entire $z = 0$ plane. This result, known prior to any actual calculation, can profitably be utilized to facilitate the mathematics of $H$-polarization solutions. It may also explain why rather more analytical model calculations have been carried out in the past for $H$-polarization [12], [13] than for $E$-polarization, where there is no such *a priori* knowledge about any of the field components at the surface. However, to render calculations more tractable and in analogy with the $H$-polarization situation, some early $E$-polarization studies (cf. Weaver [8] and Fischer [9]) did postulate a uniform horizontal magnetic field at the surface. Weaver and Thomson [11] later showed that this assumption does not completely invalidate the results, but can be looked upon as a first step in an interesting scheme of successive approximations proposed by Mann [14] for precisely such problems. Weaver and Thomson then calculated the second approximation of the Mann scheme and showed that the improved result agreed reasonably well with a numerical calculation by Jones and Price [10] for the model consisting of two quarter-spaces. These two papers [10], [11], as well as ones by Treumann [15] and Klügel [16] (Klügel also investigated a scheme of successive approximations and showed that the first approximation in fact overestimates the vertical field component $H_z$), were the first to give valid information about the behavior of the horizontal surface magnetic field under $E$-polarization induction, and they did show that this field can undergo appreciable variations near the conductivity discontinuity.

We should like to stress the importance of this last result from the point of view of geomagnetic observations. Assume a reference station situated on a perfectly tabular geologic structure. A coastal station some distance away but situated within the same range of a uniform inducing or primary magnetic field will display the same magnetic variations only in

its component parallel to the coast line. Both other components will display anomalous behavior. The occurrence of anomalous vertical variations was recognized early, for the simple reason that they are so very prominent at coastal or geologically perturbed locations, and almost nonexistent at good tabular sites. For horizontal components the primary variations are not cancelled by induction so that even good reference stations exhibit the well-known natural variations. It is not surprising, therefore, that the early observer did not easily become aware of the anomalous variations in the horizontal magnetic component perpendicular to shore (see, e.g., Rikitake [17]), although Schmucker [7] had quite clearly observed the anomalous decrease of the horizontal magnetic-field amplitude along profiles across the coast of California. In this case theory almost preceded observation in recognizing unequivocally that coastal stations should be the site of anomalous variations of the horizontal magnetic field component perpendicular to the coast. Strong horizontal variation anomalies are now commonly recorded not only at coastal stations but also inland (see, e.g., Camfield *et al.* [18] and especially Babour *et al.* [19]), where it is clear that large scale geologic features must be invoked to account for the observations [20].

## II. A New Model: *H*-Polarization Solution

By 1972, then, the ocean coast model consisting of two quarter-spaces could be considered as well resolved and understood, and was accounting quite satisfactorily for the actual observations. But another, perhaps slightly more realistic model was beginning to arouse interest. This is the second model depicted in Fig. 1. It consists of two perfectly uniform half-spaces, partially separated by a very thin wedge or half-plane ($y > 0, z = 0$) of infinite conductivity. Even though this ocean model is still highly idealized or artificial, especially because it fails to reproduce the gradual increase of ocean depth, it does embody the important feature of having both an ocean top ($z = -0$) and an ocean bottom ($z = +0$). It will also command interest in other problems besides the coast effect since it is a rather classical screening or diffraction problem. Here again *H*-polarization solutions [21], [22] preceded the more difficult *E*-polarization ones [23]–[24]. Nicoll and Weaver [22] in fact went beyond the Fig. 1 model to include a layer of infinite conductivity at various depths ($z > 0$), to simulate the high conductivity upper mantle of the Earth. Both *H*-polarization solutions [21], [22] are analytic and rely on the powerful Wiener–Hopf technique. Fig. 2, taken from Bailey [21], is a graphic representation of the solution. This figure takes full advantage of an interesting scaling property of the two models represented in Fig. 1. For these models, and provided one sets oneself in the quasi-static limit which neglects displacement currents (i.e., $\omega\epsilon\rho \ll 1$), and if throughout calculations one also assumes $(\omega\epsilon_0\rho)^{1/2} \ll 1$ and ignores any magnetic effects ($\mu \equiv \mu_0$), the electromagnetic-field pattern perfectly scales with the skin depth $\delta$,

$$\delta = \left(\frac{2}{\omega\mu_0\sigma}\right)^{1/2}. \tag{1}$$

For the model 1 structure one can choose for $\sigma$ in the above equation the "land-value" $\sigma_1$. The ratio $\sigma_2/\sigma_1$ then becomes a parameter of the theory. Note that this skin-depth definition is $\sqrt{2}$ times the one chosen by Baley [21]. As long as the length unit is chosen according to (1), current streamlines

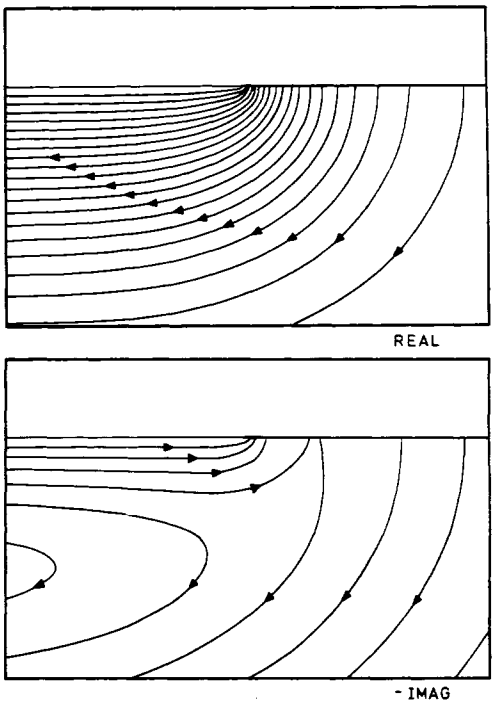


Fig. 2. Sectional view of real (in-phase) and negative imaginary (out-of-phase) current streamlines induced under *H*-polarization induction in model 2 structure of Fig. 1. The streamlines are at the same time contours where $H_x$ = const., at intervals of 0.05 $H_0$. The real contours decrease from unity at the surface, whereas the negative imaginary contours increase from zero at the surface to 0.3 for the smallest visible loop at the left. The diagram width is $2\sqrt{2}$ skin depths, as defined by (1), and the same length unit applies to the ordinate. This figure is taken from Bailey [21].

or electric field lines will maintain exactly the shape they have in Fig. 2. But lengths are not alone to scale; field amplitudes also do. Assume the uniform magnetic surface field has amplitude $H_0$. This means that the amplitude of the incident wave is $H_0/2$ for the magnetic vector, and $E_0/2$ for the electric vector, where

$$E_0/H_0 = Z_0 = (\mu_0/\epsilon_0)^{1/2} = 376.7\ \Omega \tag{2}$$

is the characteristic vacuum impedance. Then the electric surface field at ($y = -\infty, z = 0$) has amplitude $E_{-\infty y}$,

$$E_{-\infty y} = -(i\omega\mu_0\rho)^{1/2} H_0 = -(1+i) GH_0 \tag{3}$$

where

$$G = \left(\frac{\omega\mu_0\rho}{2}\right)^{1/2}. \tag{4}$$

Henceforth, we will scale all magnetic fields to the real value $H_0$. When the surface field is not uniform, as in *E*-polarization induction, we choose for $H_0$ the value of the surface field at ($y = -\infty, z = 0$). Likewise, all electric fields will henceforth be given in units of $GH_0$.

The current streamlines of Fig. 2 are simultaneously sections of surfaces on which the magnetic field is constant (we recall that only $H_x$ occurs for *H* polarization). Especially noteworthy in this figure is the rapid recovery, on the land, of the field pattern that would prevail in the absence of the ocean. At a distance of one skin-depth inland from shore, the electric surface field is affected less than 5 percent by the sea [25]. Under the ocean, however, the field pattern is quite interest-

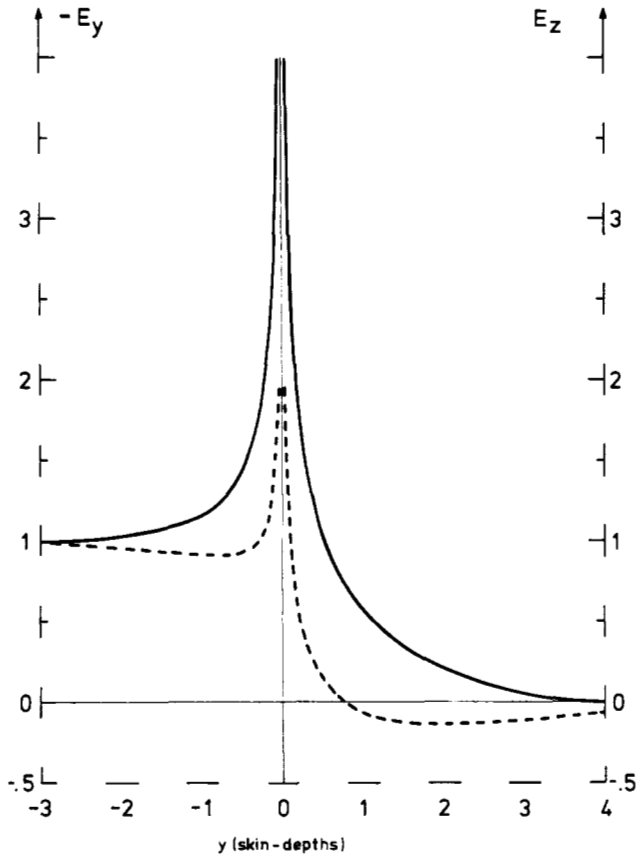


Fig. 3. $H$-polarization induction in model 2 of Fig. 1. For $y < 0$ this diagram represents Re $E_y$ (full line) and Im $E_y$ (dashed) at the $z = 0$ surface, i.e., on land. For $y > 0$ it displays Re $E_z$ (full) and Im $E_z$ (dashed) at the $z = +0$ surface, i.e., on the ocean floor. The electric fields are expressed in units of $GH_0$, given by (4), and were calculated after Bailey [21].

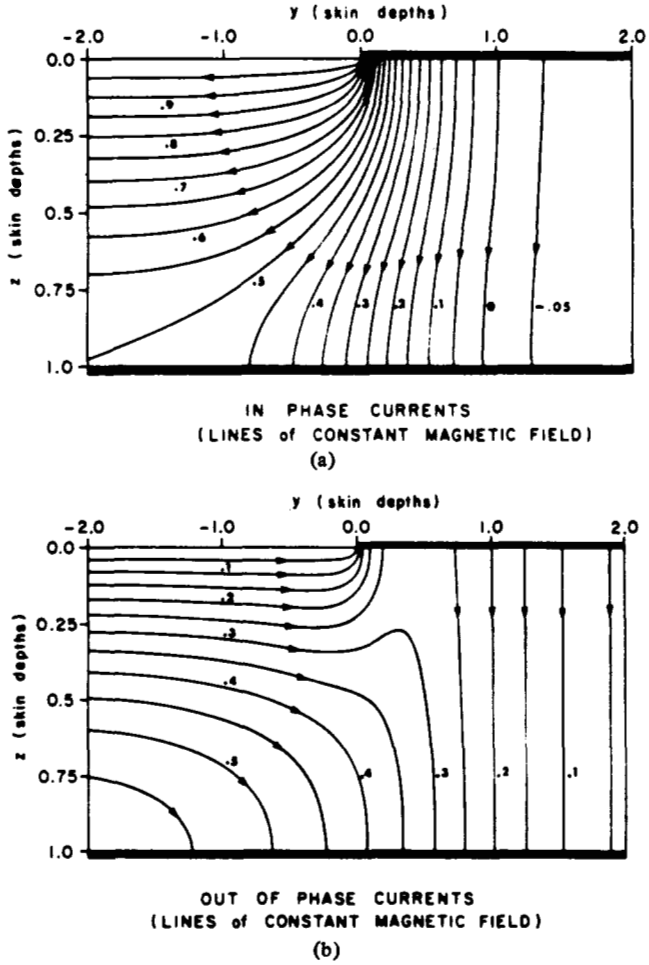


Fig. 4. Sectional view similar to Fig. 2, but with a perfectly conducting mantle at one skin depth below the surface. Note that here the length units of ordinate and abscissa are different, and that Fig. 4(b) represents the negative imaginary streamlines (i.e., the real or in-phase streamlines at the time of a quarter-period). This diagram is taken from Nicoll and Weaver [22].

ing. The very high current density at the ocean edge also leads to very high values of the electric field, as shown in Fig. 3 for the surface field components $E_y$ and $E_z$. Note that whereas $E_y$ vanishes both at the surface and at the bottom of the ocean, it tends to infinity on the land side as the ocean edge is approached. $E_z$, on the other hand, vanishes at the surface of the ocean, but increases from zero to infinity at the ocean floor as the shore is reached. On the land $E_z$ cannot completely vanish. To satisfy div $E = 0$ Price [26] has shown that surface charges will build up on the ground ($z = -0$), but that the currents and magnetic fields associated with these charges are only of order $\omega\epsilon\rho$. However, because of the singular nature of our model, $E_z$ could become quite significant near the coast [25]. Just inside the conductor ($z = +0$), the net vertical electric field vanishes, as required by the quasi-static condition div $J = 0$. Implicit in Fig. 2 is the choice of $H_0$ as phase and amplitude reference, meaning that $H_0$ is real. As a consequence the integrated current $I_y$,

$$I_y = \int_{-0}^{+\infty} dz\, J(y, z) = -H_0 \qquad (5)$$

is also real. Any imaginary current streamline coming from far away inland will, therefore, turn around and go back far into the land side, at a different depth, however [21]. Some of these streamlines, as seen in Fig. 2, are channeled partway through the sea; others turn about in the depth of the conductor.

The effect of a high conductivity mantle on the field pattern of Fig. 2 is seen in Fig. 4, taken from Nicoll and Weaver [22]. Figs. 5 and 6, from the same authors, show the behavior of the electric field at the surface of land and of the magnetic field at the ocean bottom for various mantle depths $D$ expressed in units of the skin depth $\delta$, defined in (1). It is interesting to observe in Fig. 4 how both in-phase and out-of-phase currents flow almost vertically from ocean to mantle or vice versa. This behavior should become even more marked when the mantle depth decreases, and this seems to be the most striking difference with Fig. 2. Noteworthy in Fig. 5 is the slight decrease of electric field amplitude in the range of very deep mantles [22]. This agrees with the oscillatory behavior of two layer systems when the first layer is thicker than $\pi/4$ times its own skin depth (cf. equation (1) and see, e.g., Keller and Frischknecht [27]). In Fig. 6 we note that the magnetic field at the sea floor appears to become insensitive to mantle depth when that depth becomes smaller than a tenth of a skin depth. Discontinuity of $H_x$ across the perfect surface conductor ($y > 0$, $z = 0$) arises, of course, because of the finite total current carried by that perfect conductor.

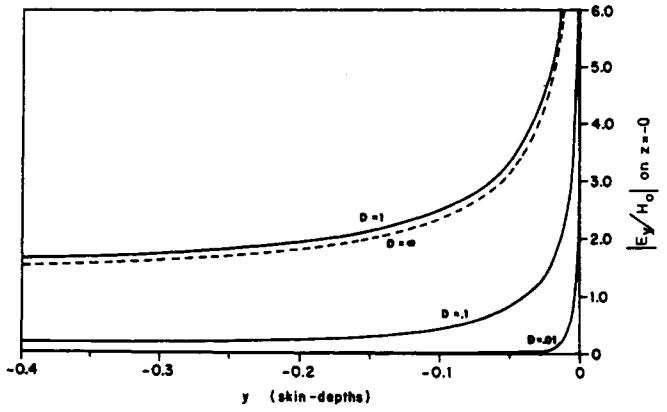


Fig. 5. Variation under $H$-polarization induction of the magnitude $|E_y|$ of the electric field along the surface, for various depths $D$ of a perfectly conducting mantle. The ordinate unit is $G$, as per (4). The dashed curve corresponds to model 2 of Fig. 1. This diagram is reproduced from Nicoll and Weaver [22].

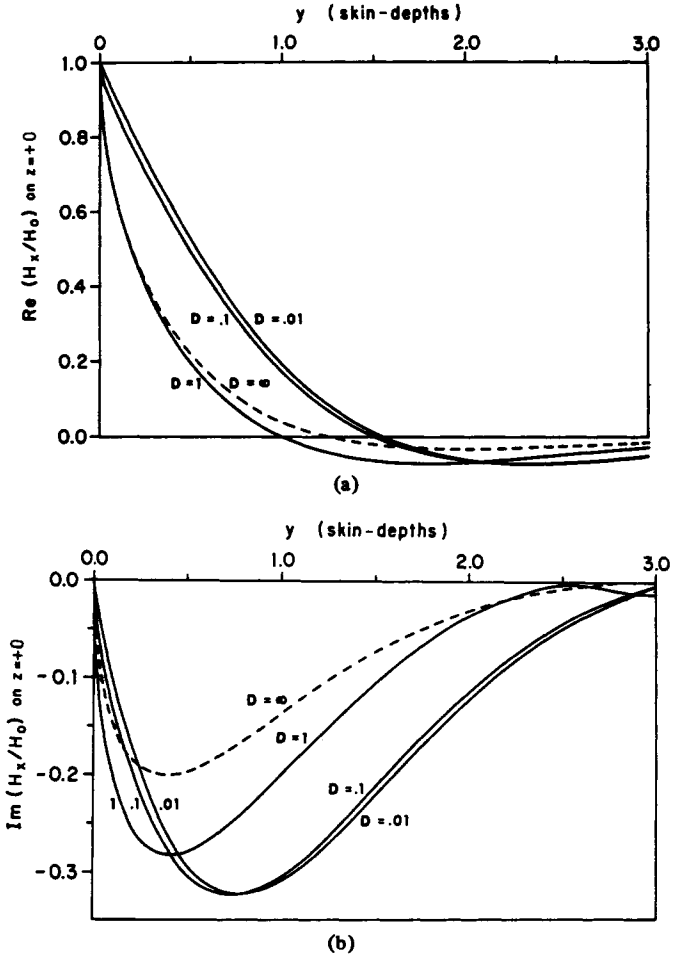


Fig. 6. Variation under $H$-polarization induction of the magnetic field $H_x$ at the ocean floor, for various depths $D$ of a perfectly conducting mantle. (a) Real part of $H_x$. (b) Imaginary part of $H_x$. The dashed curves corresponding to model 2 of Fig. 1. This diagram is reproduced from Nicoll and Weaver [22].

## III. A New Model: $E$-Polarization Solution

Whereas the $H$-polarization solution of the second model represented in Fig. 1 was successfully carried out by the Wiener-Hopf method, this method appeared less suitable to attack the $E$-polarization problem. Here a Green's function

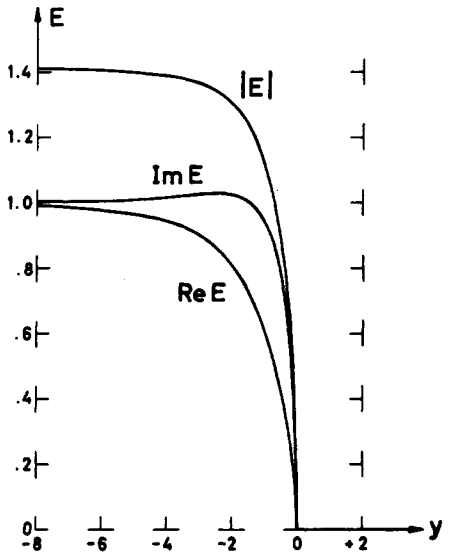


Fig. 7. The electric field $E = E_x$ at the $z = 0$ surface for $E$-polarization induction in the model 2 structure of Fig. 1, according to [24]. The ordinate unit is $GH_0$ as per (4), and the abscissa is given in skin depths, as per (1).

approach [23], [24] seemed more appropriate. The integration volumes chosen are the two half-spaces $z < 0$ and $z > 0$. Using the technique of "image sources" a Green's function $G(r, r')$ can be constructed which vanishes when either $r$ or $r'$ are on the $z = 0$ boundary. It is then possible to derive expressions which give the electric field anywhere in terms of this field on the $z = 0$ surface. This surface field is derived from the continuity of the horizontal magnetic field $H_y$ across the land surface ($y < 0$, $z = 0$). The perfect conductor sheath at ($y > 0$, $z = 0$) can again carry a finite integrated current over a vanishing thickness. In this polarization, therefore, it is $H_y$ that will be discontinuous across the $z = 0$ interface for $y > 0$. The field at the top ($z = -0$) will correspond to what is expected at the ocean surface, and the field below the sheath ($z = +0$) represents what is expected at the ocean floor. What the required continuity of $H_y$ at $y < 0$, $z = 0$ yields is an integral equation for $E(y)$, which we define as electric field $E_x$ at the $z = 0$ interface. This integral equation can probably not be solved analytically, but it is worth stressing that up to the point we have now reached in our description, the solution proposed by Fischer *et al.* [23], [24] is analytic and perfectly rigorous, and in fact allows for magnetic effects ($\mu \neq \mu_0$ but uniform in the conductor) and even includes displacement currents. This should prove of interest for the study of high-frequency effects. From here, final resolution can be achieved by solving the integral equation numerically. The numerical $E(y)$ data so obtained is then used to calculate all other field parameters.

For the nonmagnetic and quasi-static limit, with the scaling properties discussed in the previous section, the surface field $E(y)$ takes the form shown in Fig. 7, obviously satisfying the conditions of continuity of tangential fields. We recall that magnetic- and electric-field amplitudes are scaled to real units given by $H_0 = H_y(y = -\infty, z = 0)$ and $GH_0$, respectively, where now $E_{-\infty x} = E_x(y = -\infty, z = 0) = (1 + i)\, GH_0$. The electromagnetic field configuration throughout the structure is shown in Fig. 8. Here the pattern is simultaneously one of magnetic lines of force and of sections of surfaces on which

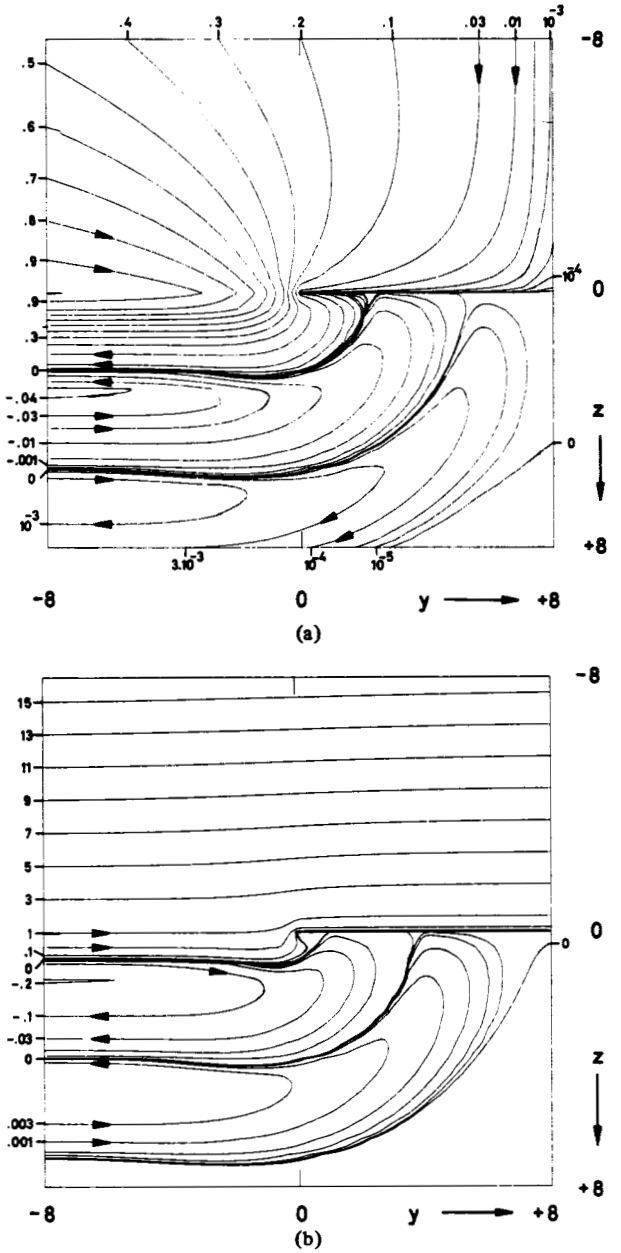


Fig. 8. Computer plots of the field-pattern in model 2 structure of Fig. 1, reproduced from [24]. These diagrams are cross sectional views of a 16 × 16 skin depths square of (a) the real and (b) the imaginary $E$ = const. Surfaces. The contour parameters are in units of $GH_0$, as per (4), and simultaneously represent (a) imaginary and (b) real magnetic field lines. A correct picture of the field-line density obtains only in the regions with a uniform contour interval.

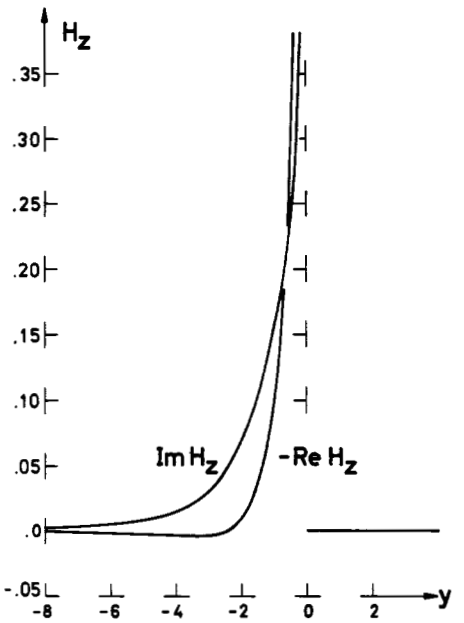


Fig. 9. Vertical magnetic field $H_z$ at the $z = 0$ surface under $E$-polarization induction in the model 2 structure of Fig. 1, according to [24]. The ordinate units is $H_0$ and the abscissa is given in skin-depths, as per (1).

the electric field amplitude assumes a constant value, expressed by the label of the line. Because the dimensions of these diagrams extend over an area of 16 × 16 skin depths, much larger than the corresponding $H$-polarization diagrams (Fig. 2), it is easy to recognize the nodes of both electric and magnetic fields of the attenuated wave pattern inside the conductor. Especially noteworthy in Fig. 8(a) is the great range of distances in the medium of incidence over which the field pattern is affected by the presence of the ocean coast. Because the electric field must vanish everywhere on the perfectly conducting sheath, it follows from Maxwell's equations that no magnetic field line can enter the sheath. Everywhere at the top and bottom surfaces of the model ocean the magnetic field lines are tangential. The main consequence of this is that these field lines must turn around the ocean edge in a bundle which reaches enormous densities. At the edge itself the field-line concentration goes to infinity, and we therefore expect the following field components also to increase toward infinity at the edge:

$$\begin{cases} H_z(y \longrightarrow -0, z = 0) \\ H_y(y \longrightarrow +0, z = 0). \end{cases} \tag{6}$$

Our data, represented in the graphs of Figs. 9 and 10, suggest that these two field components tend to infinity as $|y|^{-1/2}$, in accordance with the behavior found by Weidelt [28] for a related thin sheet problem, and with Meixner's well-known edge condition [29]–[31]. The present result is of interest because it corresponds to a system of two conducting wedges ($\sigma$ finite, $\theta = 180°$, and $\sigma \to \infty$, $\theta = 0$) and a dielectric wedge ($\sigma = 0$, $\theta = 180°$). Intimately related with this behavior of the magnetic field are ocean currents $I(y)$ which also grow out of all bounds when $y \to +0$. These currents (per unit length of the perfect sheath conductor) are given by

$$I(y) = H_y(y, z = -0) - H_y(y, z = +0) \tag{7}$$

and are also represented in Fig. 10.

While the horizontal magnetic field $H_y$ at the surface of the land remains finite all the way to the ocean coast, Fig. 10 shows that it does vary strongly near the edge, and even far inland appreciable variations are observed. However, such strong variations, just as the growth to infinity of fields and current $H_z$, $H_y$, and $I$, are a direct consequence of the unrealistic abruptness of our ocean coast model. In a more realistic situation the magnetic field lines are not totally prevented from penetrating the ocean, and can turn around the edge in the shallower parts of the water. $H_z$, $H_y$, and $I$ will probably still vary quite strongly on the ocean side, but on the land $H_y$

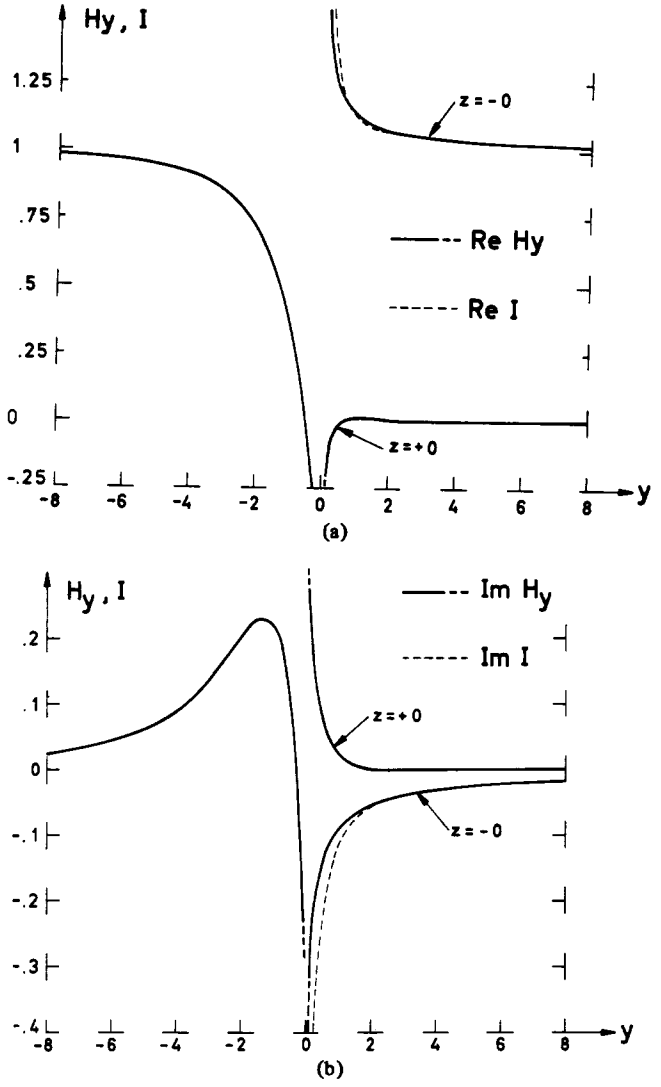


Fig. 10. Horizontal magnetic field $H_y$ at the $z = 0$ surface under $E$-polarization induction in the model 2 structure of Fig. 1, according to [24]. The ordinate unit is $H_0$ and the abscissa is given in skin depths, as per (1). For $y < 0$ diagrams (a) and (b), respectively, represent real and imaginary parts of $H_y$ on the land. For $y > 0$ these same diagrams give $H_y$ at the ocean surface ($z = -0$) and at the ocean floor ($z = +0$), as well as the integrated ocean current $I(y)$ calculated with (7).

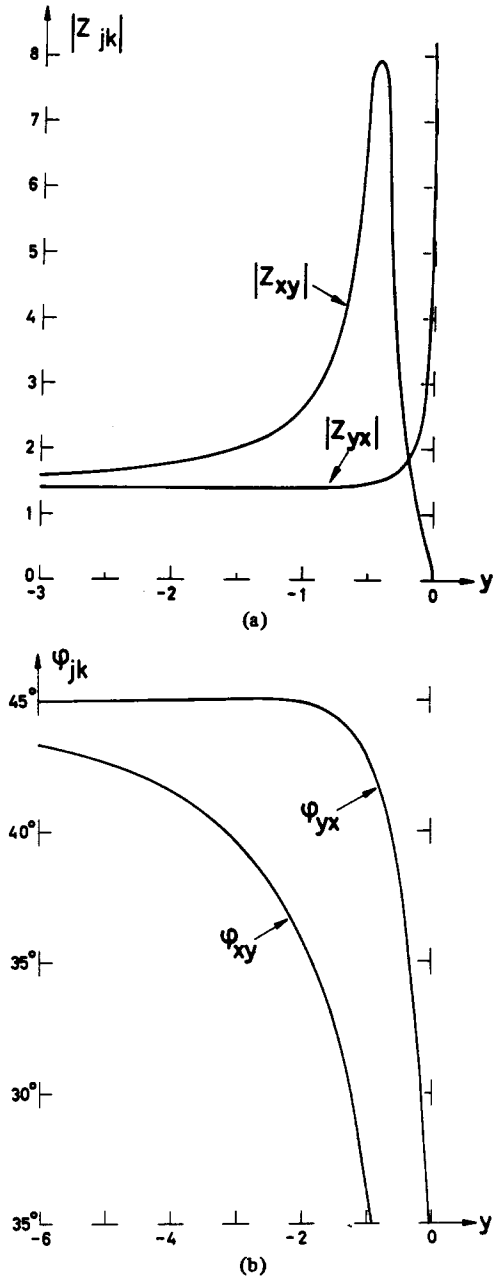


Fig. 11. Surface impedance modulus (a) and phase (b) for the model 2 structure of Fig. 1, according to [24]. The index pair $xy$ refers to $E$-polarization and the pair $yx$ to $H$-polarization. The ordinate is given in units of $G$ as per (10), and the abscissa is given in skin depths defined with (1). Note how much further inland the ocean affects $Z_{xy}$ than $Z_{yx}$. But whereas $Z_{xy}$ remains finite and vanishes at the coast, $Z_{yx}$ goes to infinity right at ocean edge.

may, as often observed, exhibit only a weak departure from its constant value $H_0$ far inland, which we take as reference.

## IV. The Magnetotelluric Surface Impedance

Impedance measurements under conditions of induction by natural phenomena, i.e., caused by geomagnetic variations, are of course most easily carried out on land. This may explain why they are usually given the special name "magnetotelluric impedance." On top and at the bottom of our idealized ocean the impedance vanishes, which of course is not quite realistic. Today, there are several active research projects involving impedance measurements at sea. We shall not be concerned with these here, but will return to our model calculations.

The magnetotelluric surface impedance is of special interest to the geomagneticist or prospector because it is the ratio of two fields which can easily be measured; horizontal electric and magnetic fields at ground level. Since this impedance relates two-component vectors, it is a tensor. For 2-D structures and when coordinates are aligned with the structural features of symmetry, however, only two of the tensor elements are nonzero [32]. Here, these two impedance elements relate to the two polarizations, namely,

$$Z_{yx}(y) = -\frac{E_y(y)}{H_x(y)} = |Z_{yx}(y)| \exp[i\varphi_{yx}(y)],$$

for $H$-polarization (8)

and

$$Z_{xy}(y) = \frac{E_x(y)}{H_y(y)} = |Z_{xy}(y)| \exp[i\varphi_{xy}(y)],$$

for $E$-polarization. (9)

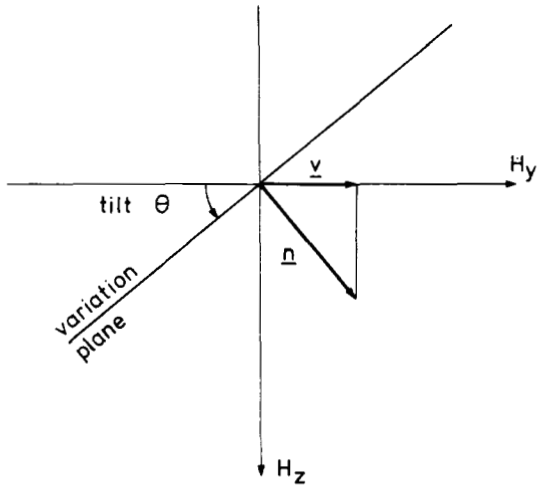


Fig. 12. Cross sectional view of a variations plane in the idealized situation when $H_z$ and $H_y$ variations are strictly in phase. This diagram also serves to define the angle of tilt $\theta$ and Parkinson's induction arrow $\boldsymbol{v}$ [3], [4].

Throughout this paper, we have set ourselves in the frequency domain, and the above impedances in particular are defined only in the frequency domain. Again we scale these impedances to their value at $(y = -\infty, z = 0)$, where they become identical and obtain, according to (3), the value $Z_{-\infty}$,

$$Z_{-\infty} = (1 + i)\, G = (1 + i)\left(\frac{\omega\mu_0\,\rho}{2}\right)^{1/2}. \tag{10}$$

When expressed in units of $G$ the two impedances $Z_{yx}(y)$ and $Z_{xy}(y)$ behave as shown in Fig. 11 (cf. also [25]).

As was to be expected after what we have seen so far, the most striking feature of Fig. 11 is the much larger range of distances inland to which the presence of the ocean is felt under $E$-polarization induction than $H$-polarization. If we take as range the point where the modulus has reached a value of 2 $G$, then the $E$-polarization range is over an order of magnitude larger than the $H$-polarization one. A range ratio of 5 or more is obtained when equal phase departures are considered. It is interesting to observe that for both polarizations the phase response seems to be affected further inland than the amplitude response, but phase may be more difficult to measure accurately than amplitude.

The cause of the much greater range to which the coast effect is carried inland for $E$-polarization than for $H$-polarization has been discussed in detail elsewhere [24]; it resides in the extremely large currents that flow parallel to shore at the ocean coast. In our model these currents grow out of all bounds right at the ocean edge and therefore act as a very long line antenna carrying a finite emission current. No such antenna effect occurs for $H$-polarization. As a consequence, $E$-polarization is much more effective than $H$-polarization response in locating distant anomalies. But this long range can also render $E$-polarization inappropriate to detect a strip of high resistivity material squeezed between two regions of good conductivity, or vice versa. Across the high resistivity strip the electric field amplitude does not succeed in rising much above its low value at the surface of the two good conductors. Here $H$-polarization offers a much more sensitive tool, since the electric field, and, therefore, also the surface impedance, can rise very sharply to large amplitudes within the strip, as seen, for example, in related studies by Geyer [33], and Wait and Spies [34].

## V. Parkinson's Induction Arrow

Parkinson [3]–[5] (see also Wiese [6]), who discovered the directional character of the ocean coast effect after studying a large number of events, proposed a convenient arrow or vector representation of the effect. Assume for a moment that $H_x$, $H_y$, and $H_z$ all vary at the same frequency. Since $H_y$ is correlated with $H_z$ their phase relationship will be stable, whereas in an ensemble of events the phase of $H_x$ will be distributed statistically. If we assume, at first, that $H_y$ and $H_z$ are exactly in phase the extremity of the variation vector $H(t)$ will describe a plane. Referring to the coordinates of Fig. 1, this plane will be perpendicular to the figure. If for a while we continue to disregard the phase, we get the field configuration shown in Fig. 12, in which the variation plane is also indicated. In this situation Parkinson [3], [4] defined his induction arrow as the horizontal projection of the *downgoing* unit normal vector to that plane. As in Fig. 12, this arrow is seen to point toward the sea. With reference to Fig. 12, Parkinson's arrow $\boldsymbol{v}$ has an amplitude $v$ given as

$$v = \sin\theta \tag{11}$$

where

$$\tan\theta = \frac{-H_z}{H_y} \tag{12}$$

and the convention is adopted that $v$ is positive when $H_y$ and $-H_z$ have the same sign (the need for a negative sign in front of $H_z$ arises because our $z$-axis points downward, unlike Parkinson's [4]). This is obviously an ambiguous convention when $H_y$ and $-H_z$ are not nearly in-phase or 180° out-of-phase, since their amplitudes may then always be considered as positive. But the most significant feature emerging from this definition of the arrow $\boldsymbol{v}$, is that it does not, for truly 2-$D$ structures, involve component $H_x$.

Let us now generalize (11) and (12) to take account of the phase relationship between $H_y$ and $-H_z$, writing

$$\tan\theta_1 + i\tan\theta_2 = \frac{-(\operatorname{Re} H_z + i \operatorname{Im} H_z)}{\operatorname{Re} H_y + i \operatorname{Im} H_y}. \tag{13}$$

We then define the in-phase and out-of-phase arrows, respec-

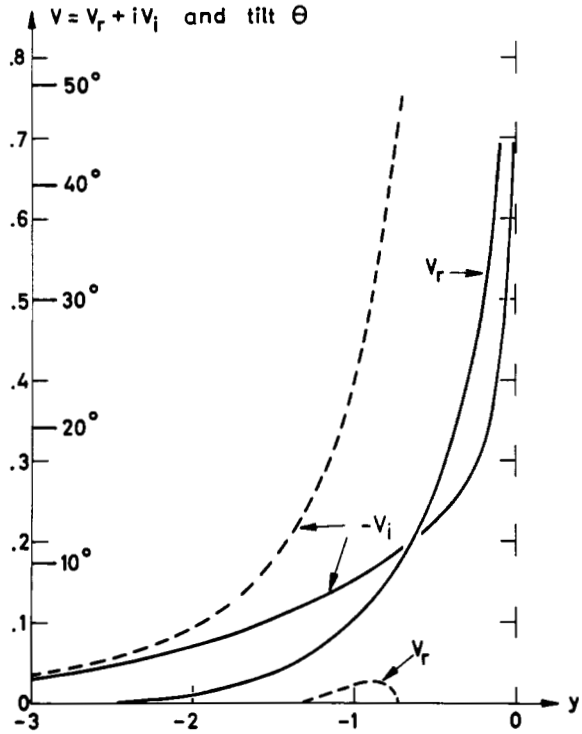


Fig. 13. Real and imaginary induction arrows $v_r$ and $v_i$, and angles of tilt $\theta_{1,2}$, calculated for the model 2 structure of Fig. 1. The dashed curves are obtained when the horizontal variations $H_y$ are those represented in Fig. 10. The full curves are found when $H_y$ is replaced by the reference field $H_0$ at ($y = -\infty$, $z = 0$). Note that $v_r > 0$ means an arrow directed toward the ocean, whereas $v_i < 0$ points inland.

tively as [35]

$$v_r = \sin\theta_1 \quad \text{and} \quad v_i = \sin\theta_2. \tag{14}$$

When we compute $v_r$ and $v_i$ in this manner we obtain the dashed curves of Fig. 13. Whereas $v_i$ has the qualitative behavior observed in practice, something obviously went wrong with $v_r$ which should be found large and positive (i.e., pointing toward the sea). The reason $v_r$ comes out wrong lies in the far too extreme features of our ocean coast model, which produces variations of $H_y$ that go far beyond what is usually observed. If instead of $H_y$ we introduce the reference field $H_0$ into (13), we obtain the full lines of Fig. 13, in excellent agreement with observations at or near ocean coasts [7], i.e., a real or in-phase arrow pointing towards the high conductivity medium and an imaginary or out-of-phase arrow pointing away from it. As claimed by Schmucker [7a], the out-of-phase arrow is particulary strong when the conductivity anomaly is close to the surface; this is especially true here. Also in excellent agreement with observations is the range of distances from the coast over which a significant arrow amplitude is observed [7], i.e., about one skin depth or 300 km for $\rho = 100\ \Omega$m and periods of one cycle per hour.

## VI. Range of the Ocean Coast Effect

In our discussion of the surface impedance (Section IV) and of the induction arrow (Section V) we have pointed out the comparatively long and short ranges of the coast effect observed on land for $E$- and $H$-polarization, respectively. It is interesting also to compare these ranges over the ocean surface and at the sea floor. For our idealized ocean model the range over the water is zero, since the electric field vanishes and the surface magnetic field $H_x$ is horizontal and uniform. For $E$-polarization the surface impedance also vanishes and the surface magnetic field too is purely horizontal; but it is not uniform and indeed, as seen in Fig. 10, it varies strongly near the shore over a range of approximately one or two skin depths [25]. On the ocean floor $H$-polarization induces an $E_z$ and an $H_x$ component, both of which remain appreciable (i.e., about 10 percent of $E_{-\infty y}$ and $H_0$, respectively) up to distances of over a skin-depth from shore. With $E$-polarization the induced $H_y$ drops very quickly from its infinite value, $-\infty(1+i)$ at the coast, to about 10 percent of $H_0$ at half a skin depth from the shore. Here, for once, $H$-polarization produces effects that reach further than $E$-polarization. This probably arises because with $H$-polarization current can flow from the mantle into the ocean (cf. Fig. 2), whereas with $E$-polarization the corresponding magnetic field-lines are bent around the model ocean edge (cf. Fig. 8).

The long range of $E$-polarization induction, found both on land and on the ocean surface of our model, is significant in relation to electromagnetic sounding or surveying quite generally. As an example we mention a recent magnetotelluric profile carried out in Iceland across the mid-Atlantic ridge [36]. The upwelling ridge material has a rather low resistivity of about 80 $\Omega$m and forms a segment of about 90 km width. On both sides of this segment are high resistivity plates of about 1000 $\Omega$m and thicknesses of a few tens of kilometers. Although this structure is not of a sea-coast type, it furnishes a beautiful example of the large difference in the ranges of $E$- and $H$-polarization effects. For periods from 10 to 1000 s, corresponding to skin depths of 14 and 140 km, respectively,

in the high conductivity segment, the $H$-polarization apparent resistivity drops quite abruptly from a high value of about 1000 Ωm or more on the plates to a low of 80 Ωm in the segment. With $E$-polarization, the low apparent resistivity of 80 Ωm in the segment does not rise as one moves onto the high resistivity plates, but remains at the low segment value for distances of well over 50 km from the plate edge. This is not surprising, as 50 km is a rather short distance compared to the skin depth of the high resistivity plates: 50 km at 10 s and and 500 km at 1000 s periods. This example also demonstrates that $H$-polarization measurements, while very sensitive to perturbations at very close range, are much less perturbed by distant lateral inhomogeneities and will, therefore, generally yield a truer picture of the ground conditions *at the point of observation.*

## VIII. Conclusions

We have seen that present model calculations furnish a rather good understanding of geomagnetic effects observed near ocean coasts. These calculations also shed light on electromagnetic characteristics of 2-$D$ geologic structures in general, particularly when large lateral conductivity contrasts are present. Refinements are expected from calculations with more realistic ocean models, as for example a highly conducting wedge, or curved coastlines. Even greater improvements can be expected from a model in which the ocean is represented by a surface sheath of variable integrated conductivity that can simulate the gradual increase of ocean depth. Such models, which are presently analyzed numerically by Weaver and co-workers [37], should avoid the unrealistic abruptness of our ocean coast model and be capable of explaining the behavior of all the fields, in particular also the horizontal electric fields at the surface and the bottom of the sea. Because of the singularity connected with the apex of a wedge, analytic rather than numerical solutions would be desirable. Such improvements may help to dispel fully misgivings of the sort expressed by Bullard and Parker [1] concerning our understanding of the ocean coast effect and render unnecessary their assumption that the upper mantle, at depths of some hundreds of kilometers, is very different under oceans than under continents.

Parkinson [38] has pointed out that there are situations where (but at much shallower depths) a significant difference for the conductivities beneath the ocean and beneath the continent must be expected. In a tectonic area like Western Canada, the two resistivities of around 20 Ωm are probably little different. But in Western Australia, a shield area, the conductivity is probably very much lower beneath the continent. According to Parkinson [38] our Fig. 11 fits the Canadian data far better than the Australian.

## Acknowledgment

The author is grateful to Dr. Weaver, Dr. Schumucker, and Dr. Parkinson for reading the manuscript and for some useful suggestions.

## References

[1] E. C. Bullard and R. L. Parker, "Electromagnetic induction in the oceans," in *The Sea*, A. E. Maxwell, Ed. New York: Wiley, 1970, vol. 4, pp. 695–730.

[2] A. A. Ashour, "Theoretical models for electromagnetic induction in the oceans," *Phys. Earth Planet. Int.*, vol. 7, pp. 303–312, 1973.

[3] W. D. Parkinson, "Directions of rapid geomagnetic fluctuations," *Geophys. J. Roy. Astron. Soc.*, vol. 2, pp. 1–14, 1959.

[4] W. D. Parksinon, "The influence of continents and oceans on geomagnetic variations," *Geophys. J. Roy. Astron. Soc.*, vol. 6, pp. 441–449, 1962.

[5] W. D. Parkinson, "Conductivity anomalies in Australia and the ocean-effect," *J. Geomag. Geoelect.*, vol. 15, p. 222–226, 1964.

[6] a) H. Wiese, "Geomagnetische Tiefentellurik Teil II: Die Streichrichtung der Untergrundstrukturen des elektrischen Widerstandes, erschlossen aus geomagnetischen Variationen," *Geofis. Pura. Appl.*, vol. 52, pp. 83–103, 1962.
b) ——, "Geomagnetische Tiefentellurik Teil III: Die geomagnetischen Variationen in Mittel- und Südost-Europa als Indikator der Streichrichtung grossräumiger elektrischer Untergrundstrukturen," *Geofis. Appl.*, vol. 56, pp. 101–114, 1963.
c) ——, "Geomagnetische Tiefentellurik," *Deutsche Akad. Wiss. Berlin, Geomagn. Inst. Potsdam.*, Abh. No. 36, 146 pp. 1965.

[7] U. Schmucker, "Anomalies of geomagnetic variations in the southwestern United States"; a) *Bull. Scripps Inst. Oceanography*, vol. 13, Univ. of California Press, 1970; b) *J. Geomag. Geoelect.*, vol. 15, pp. 193–221, 1964.

[8] J. T. Weaver, "The electromagnetic field within a discontinuous conductor with reference to geomagnetic micropulsations near a coastline," *Can. J. Phys.*, vol. 41, pp. 484–495, 1963.

[9] G. Fischer, "Microwave surface impedance of a periodic medium," *J. Math. Phys.*, vol. 5, pp. 1158–1167, 1964.

[10] F. W. Jones and A. T. Price, "The perturbations of alternating geomagnetic fields by conductivity anomalies," *Geophys. J. Roy. Astron. Soc.*, vol. 20, pp. 317–334, 1970.

[11] J. T. Weaver and D. J. Thomson, "Induction in a non-uniform conducting half-space by an external line current," *Geophys. J. Roy. Astron. Soc.*, vol. 28, pp. 163–185, 1972.

[12] I. d'Erceville and G. Kunetz, "The effect of a fault on the Earth's natural electromagnetic field," *Geophysics*, vol. 27, pp. 651–665, 1962.

[13] C. R. Brewitt-Taylor, "A model for the coast effect," *Phys. Earth Planet. Int.*, vol. 10, pp. 151–158, 1975. (This paper was first presented at the 2nd Workshop Electromagnetic Induction in the Earth, Ottawa, Canada, 1974. *See also:* "A model for the sea-floor coast effect in $H$-polarization–further results," *Phys. Earth Planet. Int.*, vol. 13, pp. 9–14, 1976.

[14] J. E. Mann, Jr., "A perturbation technique for solving boundary value problems arising in the electrodynamics of conducting bodies," *Appl. Sci. Res.*, vol. 22, pp. 113–126, 1970.

[15] R. Treumann, "Magnetic field behaviour near conductivity discontinuities and possible inferences from geomagnetic local gradients," *Phys. Earth Planet. Int.*, vol. 1, pp. 148–150, 1968.

[16] M. Klügel, "Induction in plates with two-dimensional conductivity distribution," Acta Geodaet. Geophys. et Montanist., Hungary, vol. 12, pp. 267–273, 1977. (This paper was first presented at 3rd Workshop Electromagnetic Induction in the Earth, Sopron, Hungary, 1976.)

[17] T. Rikitake, "Some characteristics of geomagnetic variation anomaly in Japan," *J. Geomag. Geoelect.*, vol. 17, pp. 95–97, 1965.

[18] P. A. Camfield, D. I. Gough, and H. Porath, "Magnetometer array studies in the north-western United States and south-western Canada," *Geophys. J. Roy. Astr. Soc.*, vol. 22, pp. 201–221, 1970.

[19] K. Babour, J. Mosnier, M. Daignieres, G. Vasseur, J. L. Le Mouël, and J. C. Rossignol, "A geomagnetic variation anomaly in the northern Pyrenees," *Geophys. J. Roy. Astron. Soc.*, vol. 45, pp. 583–600, 1976.

[20] G. Vasseur and P. Weidelt, "Bimodal electromagnetic induction in non-uniform thin sheets with an application to the northern Pyrenean induction anomaly," *Geophys. J. Roy. Astron. Soc.*, vol. 51, pp. 669–690, 1977.

[21] R. C. Bailey, "Electromagnetic induction over the edge of a perfectly conducting ocean: the $H$-polarization case," *Geophys. J. Roy. Astron. Soc.*, vol. 48, pp. 385–392, 1977. (This paper was first Presented at the 2nd Workshop on Electromagnetic Induction in the Earth, Ottawa, Canada, 1974.)

[22] M. A. Nicoll and J. T. Weaver, "$H$-polarization induction over an ocean edge coupled to the mantle by a conducting crust," *Geophys. J. Roy. Astron. Soc.*, vol. 49, pp. 427–442, 1977. (A short version of this paper was first presented at the 3rd Workshop on Electromagnetic Induction in the Earth, Sopron, Hungary, 1976, and appeared in the Workshop proceedings: "Induction over an ocean edge and mantle joined by a conducting crust," *Acta Geodaet. Geophys. et Montanist*, Hungary, vol. 12, pp. 275–278, 1977.)

[23] G. Fischer, P.-A. Schnegg, and K. D. Usadel, "$E$-polarization induction in a conducting half-space screened by a perfectly conducting half-plane," *Acta Geodaet. Geophys. et Montanist.*, (Hungary), vol. 12, pp. 247–253, 1977. (Part of this paper was first presented at the 3rd Workshop on Electromagnetic Induction in the Earth, Sopron, Hungary, 1976.)

[24] G. Fischer, P.-A. Schnegg, and K. D. Usadel, "Electromagnetic

response of an ocean coast model to E-polarization induction," *Geophys. J. Roy. Astron. Soc.*, vol. 53, pp. 599-616, 1978.
[25] —, "Electromagnetic induction at a model ocean coast," *J. Geomag. Geoelect.*, in 1978.
[26] A. T. Price, "The theory of geomagnetic induction," *Phys. Earth Planet. Int.*, vol. 7, pp. 227-233, 1973.
[27] G. V. Keller and F. C. Frischknecht, *Electrical Methods in Geophysical Prospecting*. London, England: Pergamon Press, 1966.
[28] P. Weidelt, "The electromagnetic induction in two thin half-sheets," *J. Geophys. Z. Geophys.*, vol. 37, pp. 649-665, 1971.
[29] J. Meixner, "Die Kantenbedingung in der Theorie der Beugung elektromagnetischer Wellen an vollkommen leitenden ebenen Schirmen," *Ann. Phys.*, vol. 6, pp. 1-9, 1949.
[30] J. Meixner, "The behavior of electromagnetic fields at edges," *IEEE Trans. Antennas Propagat.*, vol. AP-20, pp. 442-446, 1972.
[31] J. Bach Andersen and V. V. Solodukhov, "Field behavior near a dielectric wedge," *IEEE Trans. Antennas Propagat.*, vol. AP-26, pp. 598-602, 1978.
[32] G. Fischer, "Symmetry properties of the surface impedance tensor for structures with a vertical plane of symmetry," *Geophysics*, vol. 40, pp. 1046-1050, 1975. (Part of this paper was first presented at the 2nd Workshop on Electromagnetic Induction in the Earth, Ottawa, Canada, 1974.)
[33] R. G. Geyer, "The effect of a dipping contact on the behavior of the electromagnetic field," *Geophys.*, vol. 37, pp. 337-350, 1972.
[34] J. R. Wait, and K. P. Spies, "Magneto-telluric fields for a segmented overburden," *J. Geomag. Geoelectr.*, vol. 26, pp. 449-458, 1974.
[35] The definition given here is not unique. In fact it seems that it has now become normal practice to use $v_r = tg\ \theta_1$ and $v_i = tg\ \theta_2$ (see, e.g., J. E. Everett and R. D. Hyndman, "Geomagnetic variations and electrical conductivity structure in south-western Australia," *Phys. Earth. Planet. Int.*, vol. 1, pp. 24-34, 1967, and U. Schmucker, [7] above). But this makes little difference to Fig. 13 for the smaller angles $\theta_1$ and $\theta_2$.
[36] M. Beblo and A. Bjornsson, "Magnetotelluric investigation of the lower crust and upper mantle beneath Iceland," *J. Geophys./Z. Geophys.*, vol. 45, pp. 1-16, 1979.
[37] a) J. Weaver, "Electromagnetic induction in thin sheet conductivity anomalies at the surface of the earth," this issue, pp. 1044-1050.
b) V. R. Green and J. T. Weaver, "Two-dimensional induction in a thin sheet of variable integrated conductivity at the surface of a uniform conducting earth," *Geophys. J. Roy. Astron. Soc.*, vol. 55, pp. 721-736, 1978.
[38] W. D. Parkinson, private communication.

# Reconstruction Algorithms for Geophysical Applications in Noisy Environments

ROGER D. RADCLIFF, STUDENT MEMBER, IEEE, AND CONSTANTINE A. BALANIS, SENIOR MEMBER, IEEE

*Abstract*—Remote determination of underground geophysical structures is a matter of considerable interest. Detecting such structures by scanning the area of interest with electromagnetic radiation is shown to reduce to the problem of solving an inconsistent system of equations for a spatial attenuation distribution. This paper examines the employment of reconstruction algorithms to solve such systems of equations, and it presents significant modifications to a standard algorithm that vastly improves its performance in the presence of noisy data. The process of *in situ* coal gasification is taken as an example to illustrate the superior performance of the modified algorithm.

## I. Introduction

DEVELOPMENT of a system that can remotely determine the structure of various regions of the earth can have a significant impact in many areas of geophysical exploration. Such a technique would have great advantages over present methods in the search for salt and oil deposits, location of tunnels and fractures, fluid-flow monitoring, etc. Another important application is the potential to map and monitor the burn front in an *in situ* coal gasification (UCG) process. Although the techniques presented in this paper are, in general, applicable to many types of underground anomalies, the UCG process is chosen to illustrate the mathematical foundations of such a remote detection system.

Manuscript received June 6, 1978; revised November 13, 1978. This work was supported by the *In Situ* Coal Gasification Project at the Morgantown Energy Technology Center under the Department of Energy Contract EY-77-C-21-8087 (Task Order 22).

The authors are with the Department of Electrical Engineering, West Virginia University, Morgantown, WV 26506.

## II. Basic Concepts

Investigations have indicated that the electrical conductivity of gasified coal is many times greater (a factor of $\simeq 10^4$) than the conductivity of virgin coal [1]-[3]. Due to this striking difference in conductivity, regions of low conductivity in the coal seam indicate unburned coal, and regions of comparatively high conductivity designate a gasified pocket. Hence, if we can determine the electrical conductivity as a function of position everywhere in the area of interest, we have mapped the bounds of the underground coal conversion process. The data necessary to reconstruct the conductivity profile is obtained by transmission of electromagnetic waves from antennas

0018-9219/79/0700-1060$00.75 